

Signatures of Quantum Spin Liquid in Kitaev-like Frustrated Magnets

Matthias Gohlke,¹ Gideon Wachtel,² Youhei Yamaji,^{3,4} Frank Pollmann,⁵ and Yong Baek Kim^{2,6,7}

¹*Max-Planck-Institut für Physik komplexer Systeme, 01187 Dresden, Germany*

²*Department of Physics, University of Toronto, Toronto, Ontario M5S 1A7, Canada*

³*Department of Applied Physics, The University of Tokyo, Hongo, Bunkyo-ku, Tokyo, 113-8656, Japan*

⁴*JST, PRESTO, Hongo, Bunkyo-ku, Tokyo, 113-8656, Japan*

⁵*Technische Universität München, 85747 Garching, Germany*

⁶*Canadian Institute for Advanced Research/Quantum Materials Program, Toronto, Ontario MSG 1Z8, Canada*

⁷*School of Physics, Korea Institute for Advanced Study, Seoul 130-722, Korea*

Motivated by recent experiments on α -RuCl₃, we investigate a possible quantum spin liquid ground state of the honeycomb-lattice spin model with bond-dependent interactions. We consider the $K - \Gamma$ model, where K and Γ represent the Kitaev and symmetric-anisotropic interactions between spin-1/2 moments on the honeycomb lattice. Using the infinite density matrix renormalization group (iDMRG), we provide compelling evidence for the existence of quantum spin liquid phases in an extended region of the phase diagram. In particular, we use transfer matrix spectra to show the evolution of two-particle excitations with well-defined two-dimensional dispersion, which is a strong signature of quantum spin liquid. These results are compared with predictions from Majorana mean-field theory and used to infer the quasiparticle excitation spectra. Further, we compute the dynamical structure factor using finite size cluster computations and show that the results resemble the scattering continuum seen in neutron scattering experiments on α -RuCl₃. We discuss these results in light of recent and future experiments.

I. INTRODUCTION

One of the hallmarks of quantum spin liquid is the existence of fractionalized excitations¹. While it is generally difficult to detect the dispersion of single-particle excitations in fractionalized systems, the information about two-particle and other multi-particle excitations is contained in the dynamical spin structure factor measured in inelastic neutron scattering. If the ground state is a quantum spin liquid, the lower boundary of multi-particle continuum should have a well-defined dispersion. Many candidate materials for quantum spin liquid, however, do not allow such scattering experiment due to unavailability of large single crystal. Possible experiments are, therefore, quite often limited to thermodynamic measurements such as specific heat and susceptibility, as well as thermal transport. Hence it is difficult to identify smoking-gun evidence for quantum spin liquid.

In this context, recent inelastic neutron scattering experiments²⁻⁴ on α -RuCl₃ provide valuable information about multi-particle continuum in a putative quantum spin liquid material⁵. α -RuCl₃ is one of the candidate materials that support the Kitaev interaction⁶ between $j_{\text{eff}} = 1/2$ pseudo-spin moments, which is a bond-dependent frustrated Ising interaction and arises from the combination of correlation effects and spin-orbit coupling⁷⁻¹¹. When only the Kitaev interaction is present, such a model can be exactly solved⁶ and the ground state is a quantum spin liquid. On the other hand, other interactions are generally present and

they may drive a transition to a magnetically ordered state¹²⁻¹⁵.

The compound α -RuCl₃ orders magnetically at low temperatures¹⁶⁻¹⁸, possibly due to the existence of other interactions mentioned above. In spite of this, the dynamical structure factor shows a continuum of excitations at high energies both below and above the ordering temperature, which may be related to a nearby quantum spin liquid¹⁹. Elaborate *ab initio* computations indicate that the dominant exchange interactions are the Kitaev K and symmetric-anisotropic Γ interactions with small third neighbor J_3 Heisenberg interaction¹³. The dominance of K and Γ interactions is also pointed out in studies of multi-orbital Hubbard model²⁰. Furthermore, it is interesting to notice that the $K - \Gamma$ model is proposed for metal-organic frameworks with Ru³⁺ or Os³⁺ ions²¹. A previous theoretical work²² of exact diagonalization (ED) on finite size clusters suggest that the $K - \Gamma$ model may host quantum spin liquid phases in an extended region of the phase diagram and small J_3 would drive a transition to the zig-zag order that is seen in the experiment. Such a study is naturally subject to finite size effect and it is still difficult to nail down the precise nature of the ground state. In fact, the ED study mentioned above introduce a spatial anisotropy in the Kitaev interaction to avoid strong finite size effect.

In this work, we investigate the $K - \Gamma$ model using then infinite density matrix renormalization group²³⁻²⁵ (iDMRG), where the system is placed on an infinite cylinder. We first study the ground state energy, entanglement entropy, magnetization, and static struc-

ture factor for the $K - \Gamma$ model. Similar to the previous ED study, we find quantum paramagnetic ground states for ferro-like Kitaev interaction for an extended region in the phase diagram. It is also shown that the entanglement entropy in this region remains relatively high. In comparison, the entanglement entropy of a magnetically ordered state for anti-ferro-like Kitaev interaction is quite small.

In order to test the existence of coherent excitations, we compute the eigenvalues of the transfer matrix (TM) in the matrix product wavefunction. Using the mapping²⁶ between the complex eigenvalues and low-energy excitation spectra as a function of momentum, we identify the lower edge of the multi-particle excitation continuum as a function of momentum²⁷. From this, we find that the lower edge of the excitation spectra, which also corresponds to the longest correlation length in the system, moves coherently in momentum space in a well-defined fashion as a function of Γ/K . This alone tells us that these states are non-trivial and likely correspond to quantum spin liquid phases. Furthermore, the TM spectrum exhibits an emergent symmetry in its momentum dependence. Assuming that the lowest momentum-dependent eigenvalues correspond to the lower boundaries of the single- and multi-particle continuum in a quantum spin liquid, we compare the results of the transfer matrix computations and the two-particle spectra obtained in the Majorana mean-field theory for the $K - \Gamma$ model. It is found that the same symmetry which emerges in the TM spectrum is also a property of the Majorana spectrum in the mean-field theory. This suggests that the mean-field picture can capture some essential features of the two-particle excitation spectrum seen in the transfer matrix eigenvalues.

As pointed out in earlier works²⁸⁻³⁰, the dynamical spin structure factor in the Kitaev model involves not just two-particle spectra, but also the flux degrees of freedom. In fact, this makes it difficult to extract the information about the single-particle dispersion from the dynamical spin structure factor as the flux degrees of freedom may still play important roles even in the presence of the additional Γ interaction. In contrast, the transfer matrix eigenvalues computed here are directly related to the convolution of the single-particle spectra.

In order to make a more direct contact with scattering experiment, we compute the dynamical structure factor on a 24-site cluster. It is found that the low energy dynamical structure factor exhibit a star-like feature in momentum space, just like what is seen in recent neutron scattering experiments³ on α -RuCl₃. We also demonstrate that these results are consistent with the equal-time spin structure factor computed in the Majorana mean-field theory. We have further confirmed that the magnetic-field dependence of the magnetization in

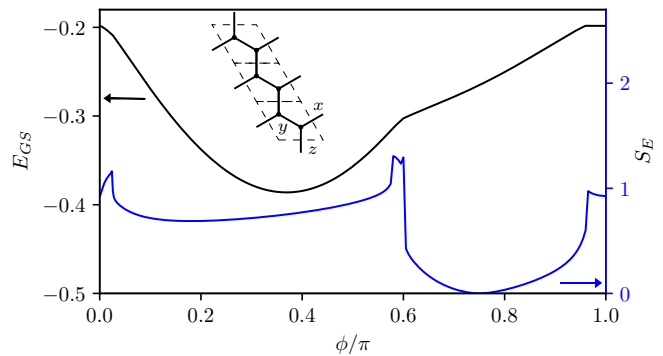


FIG. 1. Ground state energy density, E_{GS} , of the $K - \Gamma$ model, and the corresponding entanglement entropy, S_E , for a bipartition of the cylinder into two infinite cylinders, as determined using iDMRG for cylinders with circumference $L = 6$. Kinks in E_{GS} are indications of first order phase transitions. Inset shows the cylinder's three-unit-cell circumference.

the 24-site cluster is consistent with the experimental results^{15,31-37} on α -RuCl₃. Taken together, all of the results above suggest that α -RuCl₃ may be close to a quantum spin liquid described by the $K - \Gamma$ model with ferro-like Kitaev interaction.

The remainder of the paper is organized as follows. We present the model and iDMRG results in section II. In section III we present and discuss the transfer matrix (TM) spectrum. A Majorana based MFT is presented in section IV, while results of the ED calculation of the dynamic structure factor appear in section V. Details of the iDMRG and ED calculations, as well as additional results are given in the appendices.

II. iDMRG STUDY OF THE $K - \Gamma$ MODEL

The $K - \Gamma$ Hamiltonian is given by

$$\begin{aligned}
 H = & \sum_{\langle ij \rangle \in x} K_x S_i^x S_j^x + \Gamma_x (S_i^y S_j^z + S_i^z S_j^y) \\
 & + \sum_{\langle ij \rangle \in y} K_y S_i^y S_j^y + \Gamma_y (S_i^x S_j^z + S_i^z S_j^x) \\
 & + \sum_{\langle ij \rangle \in z} K_z S_i^z S_j^z + \Gamma_z (S_i^x S_j^y + S_i^y S_j^x), \quad (1)
 \end{aligned}$$

where S_i^α are spin-1/2 operators at site i of a honeycomb lattice. Unless otherwise noted, we consider here the isotropic case, $K_\alpha = K, \Gamma_\alpha = \Gamma$. Throughout the following, K and Γ are parameterized using ϕ such that $K = -\cos \phi$ and $\Gamma = \sin \phi$. We use the iDMRG method with bond dimensions of up to $\chi = 400$ to obtain the

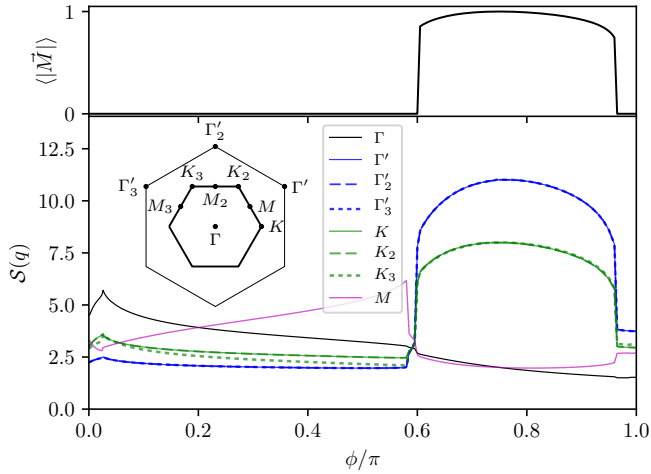


FIG. 2. Staggered magnetization (top) and static spin structure factor (bottom), calculated using iDMRG. Inset: Brillouin zone with labeled positions of symmetry points.

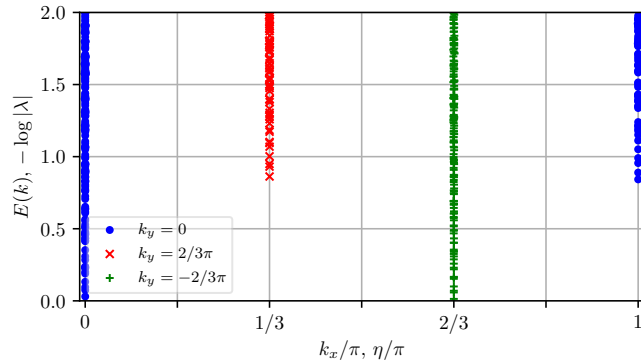


FIG. 3. Transfer matrix spectrum λ_i in the Kitaev limit ($\phi \rightarrow 0$) for $L = 6$. Plotted is the spectrum $E(k) = -\log |\lambda|$ with each point corresponding to a single eigenvalue λ , where $\lambda = |\lambda|e^{i\eta}$ and η is identified with the momentum k_x along the cylinder. k_y denotes the transverse momentum obtained as a quantum number with respect to translation along the cylinder. See App. A for more details.

ground state of this model on a narrow infinite cylinder with a three unit cell circumference ($L = 6$). In Fig. 1 we plot the ground state energy density, E_{GS} , as a function of the parameter $0 < \phi < \pi$. Starting from the ferromagnetic Kitaev limit, $\phi = 0$, E_{GS} evolves smoothly through the Γ limit, $\phi = \pi/2$. A discontinuity appears at $\phi \approx 0.6\pi$ and again slightly before the anti-ferromagnetic Kitaev limit, $\phi = \pi$. The two discontinuities are associated with a transition into, and out of, a magnetically ordered vortex state, which becomes an exact product state for $\phi = 3\pi/4$. This is evident in a plot of the entanglement entropy, S_E , also in Fig. 1, showing a vanishing S_E at this point. No-

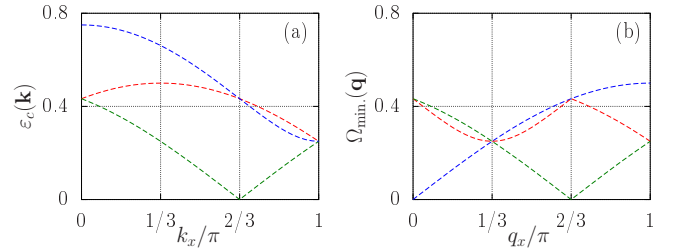


FIG. 4. (a) Single Majorana fermion spectrum $\epsilon_c(\mathbf{k})$ for the isotropic Kitaev model, $K_x = K_y = K_z = -1$, on a cylinder with a three unit cell circumference. (b) Corresponding minimum energy for two-particle excitations, $\Omega_{\min.}(\mathbf{q})$.

tice that the entanglement entropy remains as high as that of the ferro-like Kitaev limit in the entire region of $0 < \phi < 0.6\pi$. Furthermore iDMRG shows a finite staggered magnetization in $0.6\pi < \phi < 0.96\pi$, as well as an enhanced spin structure factor, Fig. 2, all consistent with a magnetically ordered phase. The main question we want to address here is: what is the nature of the ground state outside of the magnetically ordered state? The large entanglement and lack of magnetic order suggest that the ground state in this region is occupied by quantum spin liquid phases. However, a small discontinuity at $\phi \approx 0.025\pi$ in both the entanglement entropy and the spin structure factor, raises the question whether there exists a subtle transition between different kinds of spin liquid phases. To address this issue, and to gain insight into the low energy physics of the $K - \Gamma$ model as ϕ is tuned from the Kitaev to Γ limits, we turn to a detailed examination of the transfer matrix spectrum, obtained from the ground state matrix product state (MPS).

III. TRANSFER MATRIX SPECTRUM

A. The Kitaev limit

We begin by analyzing the transfer matrix spectrum, $E(k_x, k_y)$, of the pure Kitaev model, shown in Fig. 3, as a function of the momentum along the cylinder, k_x . We were also able to resolve the transverse momentum $k_y = 0, \pm 2\pi/3$, which are depicted in the figure by different colors (see Fig. 7). Here we use the demonstrated correspondence²⁶ between the complex eigenvalues of the transfer matrix and the excitation spectrum, $E(k)$. Namely, given a TM eigenvalue $\lambda_i = e^{-\epsilon_i + i\eta_i}$, the corresponding momentum (along the infinite dimension) is given by $k_i \sim \eta_i = \arg \lambda_i$, while the corresponding energy is given by $E_i \sim \epsilon_i = -\ln |\lambda_i|$ (see appendix A for details). The Kitaev model is exactly solvable in

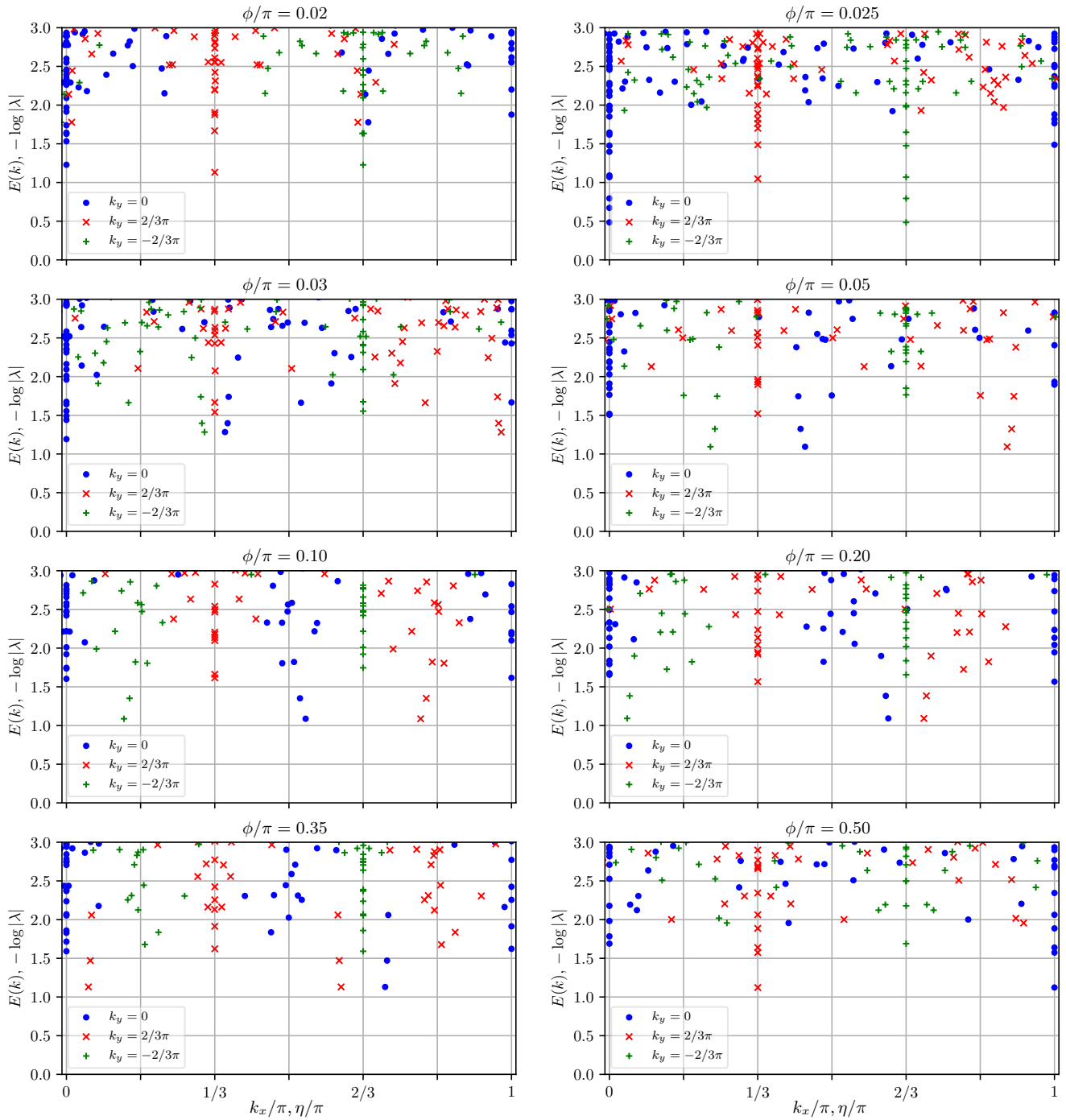


FIG. 5. Same as Fig. 3 for different ϕ .

terms of Majorana fermions, and therefore it is possible to readily identify the features in Fig. 3 with the known Majorana excitations. The most prominent feature of the Majorana spectrum, $\varepsilon_c(\mathbf{k})$, in the Kitaev

model is the existence of two gapless Dirac nodes at the corners of the Brillouin zone, $K = (2\pi/3, -2\pi/3)$ and $K' = (-2\pi/3, 2\pi/3)$ (see Fig. 4a). A continuum of excitations may thus be obtained if multiple Majorana

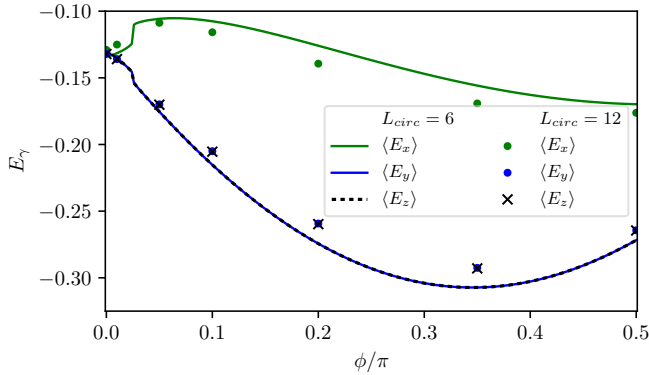


FIG. 6. Energy density per bond, as obtained using iDMRG, for systems with a three ($L = 6$) and six ($L = 12$) unit cell circumference.

fermions are excited. Fig. 4b shows the minimum excitation energies for the two particle excitation spectrum, as defined by

$$\Omega_{\min.}(\mathbf{q}) = \min_{\mathbf{k}} (|\varepsilon_c(\mathbf{q} - \mathbf{k})| + |\varepsilon_c(\mathbf{k})|). \quad (2)$$

Minima in $\Omega_{\min.}(q_x, q_y)$, as a function of q_x , in the two particle spectrum, appear at $(0, 0)$, $(\pi/3, 2\pi/3)$ and $(2\pi/3, -2\pi/3)$, which are consistent with the blue, red, and green pillars shown in Fig. 3a at these momenta. We note, however, that, at least in the pure Kitaev model, single-particle excitations seem to appear in the TM spectrum as well (see Appendix A for details).

B. The $K - \Gamma$ model

Moving away from the exactly solvable Kitaev limit, we now turn to analyze the TM spectrum of the $K - \Gamma$ model, Fig. 5, which shows the transfer matrix spectrum, $E(k_x, k_y)$, for various values of ϕ . Similarly to the Kitaev limit, minima in the continuum of excitations are clearly identified at $(0, 0)$, $(\pi/3, 2\pi/3)$, $(2\pi/3, -2\pi/3)$, and $(\pi, 0)$. All, however, are gapped. This can be understood in the context of Majorana fermions by noting that the cylindrical geometry breaks the symmetry between x bonds and y, z bonds, which in turn can lead, for $\Gamma > 0$, to anisotropic hopping amplitudes, and the gapping out of the fermions. To corroborate this point, Fig. 6 depicts the energy density per bond as a function of ϕ , displaying that indeed the symmetry between bonds is broken for $\phi > 0$.

Several additional minima appear for $\phi > 0$, with their momentum position moving as ϕ is increased. Strikingly, these additional minima seem to obey an underlying symmetry, i.e., a considerable number of eigenvalues obey $E(k_x, k_y) = E(k_x + 2\pi/3, k_y - 2\pi/3)$. For in-

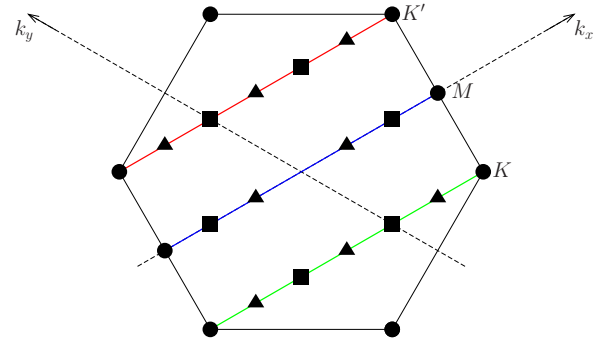


FIG. 7. Allowed momentum cuts for the cylindrical geometry. Symbols indicate the positions of the soft two-particle excitations, as deduced from the TM spectrum. ● indicate the leading soft modes at K, K' and M points. Additional soft modes are plotted for $\phi = 0.03\pi$ (▲) and $\phi = 0.2\pi$ (■). As ϕ is tuned between these values, we expect that these minima smoothly move from the squares (■) to the triangles (▲).

stance, the $\phi = 0.1\pi$ panel in Fig. 5 has a minimum near $(\pi/6, -2\pi/3)$ (green +), which has a symmetric counterpart near $(5\pi/6, 2\pi/3)$ (red x), i.e., shifted in momentum by $(2\pi/3, -2\pi/3)$. An additional counterpart is located near $(\pi/2, 0)$ (blue circle), which can be reached by inversion $\mathbf{k} \rightarrow -\mathbf{k}$, followed by the same shift in momentum. Interpreting the TM spectrum as being associated with two-particle excitations, the above symmetry suggests the existence of single-particle excitations which, in addition to inversion symmetry $\varepsilon(-\mathbf{k}) = \varepsilon(\mathbf{k})$, obey also $\varepsilon(\mathbf{k}) = \varepsilon(\mathbf{k} \pm \mathbf{K})$, where $\pm \mathbf{K}$ are the momenta at the Brillouin zone corners, K and K' , respectively. Figure 7 shows the positions of the soft two-particle excitations, for $\phi = 0.03\pi$ and $\phi = 0.2\pi$, further demonstrating the above symmetry.

In summary, the features of the TM spectrum strongly indicate that the paramagnetic phase of the $K - \Gamma$ model harbours coherent excitations commonly associated with quantum spin liquids. However, it is difficult to determine the nature of this spin liquid phase, based on the iDMRG data alone. On the one hand, the TM features suggest that in the region $0 < \phi < 0.6\pi$ the $K - \Gamma$ model harbours Majorana fermion excitations, sharing basic properties with the ground state of the ferromagnetic Kitaev model. On the other hand, the apparent transition at $\phi = 0.025\pi$ may indicate that there are two distinct spin liquid phases with a sharp transition between them. In the next section we introduce a mean-field approximation, which can be used to elucidate the above results.

IV. MAJORANA MEAN-FIELD THEORY

A. Majorana spectrum

Motivated by the iDMRG results of the previous section, we would like to formulate a Fermionic mean-field theory which closely resembles the exact solution of the Kitaev model. Therefore, following Kitaev⁶, we replace the spin operators in the Hamiltonian with products of Majorana fermion operators, $2S_i^\alpha \rightarrow ib_i^\alpha c_i$,

$$\tilde{H} = - \sum_{\langle ij \rangle \alpha \beta} K_{ij}^{\alpha\beta} ib_i^\alpha b_j^\beta ic_i c_j, \quad (3)$$

where for $\langle ij \rangle$ a z -type bond,

$$K_{ij}^{\alpha\beta} = \frac{1}{4} \begin{cases} K & \alpha = \beta = z \\ \Gamma & \alpha \neq \beta \neq z \\ 0 & \text{otherwise} \end{cases}. \quad (4)$$

Similar definitions follow for x and y -type bonds. Here, the Majorana fermion operators are normalized such that $\{b_i^\alpha, b_j^\beta\} = 2\delta_{ij}\delta_{\alpha\beta}$ and $\{c_i, c_j\} = 2\delta_{ij}$. The physical Hilbert space of the spin Hamiltonian H is then obtained by projecting the Majorana Hamiltonian \tilde{H} onto the subspace of states $|\Psi\rangle$ which obey $D_i|\Psi\rangle \equiv b_i^x b_i^y b_i^z c_i |\Psi\rangle = |\Psi\rangle$. Within a mean-field approach, we can approximate \tilde{H} with

$$H_{MF} = - \sum_{\langle ij \rangle \alpha \beta} B_{ij} K_{ij}^{\alpha\beta} ib_i^\alpha b_j^\beta - \sum_{\langle ij \rangle} A_{ij} ic_i c_j + \sum_{\langle ij \rangle} A_{ij} B_{ij}, \quad (5)$$

where the fields A_{ij} and B_{ij} obey the mean-field self-consistency equations on each bond,

$$A_{ij} = \sum_{\alpha\beta} K_{ij}^{\alpha\beta} \langle ib_i^\alpha b_j^\beta \rangle_B, \quad (6)$$

$$B_{ij} = \langle ic_i c_j \rangle_A. \quad (7)$$

Given the ground state $|\Psi_0\rangle_{MF}$ of H_{MF} , it is possible to construct an approximate ground state for H by projection onto the physical Hilbert space, $|\Psi_0\rangle \approx \prod_i (1 + D_i)/2 |\Psi_0\rangle_{MF}$.

It is straightforward to obtain a uniform, Z_2 -flux-free, solution of Equations (6) and (7), in the two-dimensional thermodynamic limit. In the following we use the convention that in A_{ij}, B_{ij} etc., the subscript i indicates a site on the odd sublattice and j a site on the even sublattice. Assuming that $A_{ij} \equiv A$ on all bonds, we obtain $B_{ij} \equiv B = 0.5248$, which is independent of A . Similarly, A is independent of B , but it does depend on the ratio K/Γ . The mean-field ground state energy per bond is given by $E_{MF} = -AB$. By solving H_{MF} , it is possible to obtain the Majorana fermion

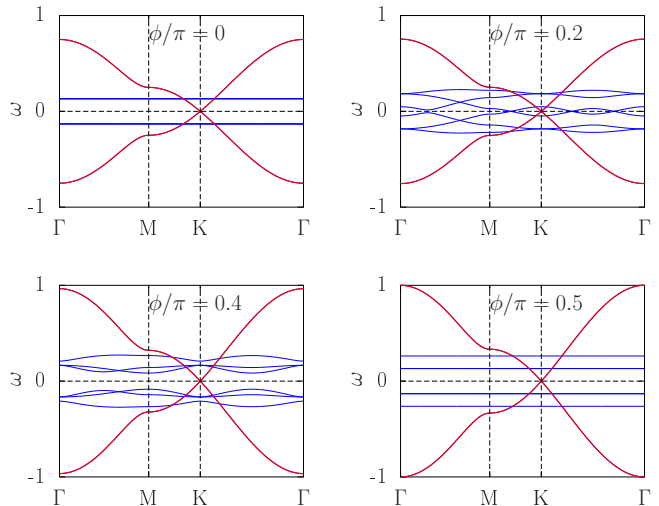


FIG. 8. Band structure of c (red) and b (blue) Majorana fermions, plotted along high symmetry lines of the Brillouin zone, for several values of ϕ in the two dimensional thermodynamic limit. The flat bands for $\phi = 0$ are three-fold degenerate; for $\phi/\pi = 0.5$, the lower energy flat bands are two-fold degenerate. When $\phi/\pi \sim 0.2$, there is a finite density of zero energy b fermion states, around the K (and Γ) points in the Brillouin zone. At $\phi/\pi = 0.4$ the b fermion bands are still dispersive, but gapped.

spectrum, shown in Fig. 8 along high symmetry lines in the Brillouin zone, for several values of ϕ . In the Kitaev limit, $\phi = 0$, one finds a single dispersing c -fermion band, with Dirac nodes at the K points of the Brillouin zone, and whose band width is set by $A = K$. Three flat bands describe the b -fermions, which are localized on the bonds. For $\phi = \pi/2$, one obtains a similarly dispersing c -fermion band, with band width $A = 4\Gamma/3$, and three flat bands which describe the b -fermions localized on the hexagons. When both K and Γ are nonzero, the b -fermions are dispersive, and become gapless in the parameter range $0.15 < \phi/\pi < 0.25$.

B. Two-Majorana spectrum

We have suggested that the TM spectrum can be associated with two-particle continua of fractionalized excitations, *some of which* obey a symmetry relation $E(k_x, k_y) = E(k_x + 2\pi/3, k_y - 2\pi/3)$. Interestingly, the Majorana mean-field Hamiltonian, Eq. (5), exhibits this symmetry for the b fermion spectrum, $\varepsilon_b(\mathbf{k}) = \varepsilon_b(\mathbf{k} \pm \mathbf{K})$ (see Appendix B for details), inducing the same symmetry in the two-particle spectrum, $\Omega_{b+c}(\mathbf{q}, \mathbf{k}) = |\varepsilon(\mathbf{q} - \mathbf{k})| + |\varepsilon(\mathbf{k})|$, as well. We note that this symmetry, $\Omega_{b+c}(\mathbf{q} \pm \mathbf{K}, \mathbf{k}) = \Omega_{b+c}(\mathbf{q}, \mathbf{k})$, holds irrespectively of the

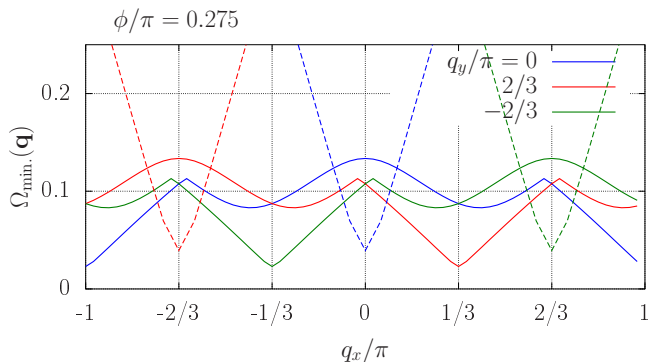


FIG. 9. $b+c$ (solid) and $c+c$ (dashed) two-Majorana fermion spectrum plotted along the three momentum cuts allowed on a cylinder with a three unit cell circumference (see fig. 7)

properties of the c -fermion spectrum. In Appendix A, we show that this is consistent with the iDMRG results, which exhibit this symmetry in the TM spectrum even when the $K - \Gamma$ coupling are anisotropic such that the minima in the c spectrum move away from the K, K' points.

Thus, the form of H_{MF} may give a good description of the fractionalized excitations, as probed by iDMRG. However, due to the strongly interacting nature of the $K - \Gamma$ model, the actual amplitudes A_{ij} and B_{ij} which should be used for such a description, as well as the value of ϕ itself, will most likely be very different from their values as determined by MFT. Nevertheless, we may still compare the MF spectra with the TM spectra, demonstrating the usefulness of H_{MF} . To do so we study the same cylindrical geometry considered above using iDMRG. As in the iDMRG calculation where the cylindrical geometry breaks the symmetry between x and y, z bonds, also here we choose different amplitudes A_{ij}, B_{ij} for different bonds. In Fig. 9 we plot the minimal energies required to excite two Majorana fermions, as given by

$$\Omega_{\min.}(\mathbf{q}) = \min_{\mathbf{k}} (|\varepsilon_{b,c}(\mathbf{q} - \mathbf{k})| + |\varepsilon_c(\mathbf{k})|), \quad (8)$$

where $\varepsilon_{b,c}(\mathbf{k})$ is the Majorana spectrum of H_{MF} . For finite anisotropy, $\varepsilon_{b,c}(\mathbf{k})$ opens a gap at all allowed momenta, and consequently, also in $\Omega_{\min.}(\mathbf{q})$. Nevertheless, the K and K' points remain soft, as in the TM spectrum. Furthermore, additional soft modes appear at finite Γ in the $b+c$ spectrum, which obeys the symmetry $\Omega_{\min.}(\mathbf{q} \pm \mathbf{K}) = \Omega_{\min.}(\mathbf{q})$. For example, shifting the solid green curve ($q_y = -2\pi/3$) in Fig. 9 by $q_x = 2\pi/3$, yields the solid red curve ($q_y = 2\pi/3$). By demonstrating this symmetry, we conclude that H_{MF} may give a good description of the low energy excitations of the $K - \Gamma$ model, as seen in the TM spectrum.

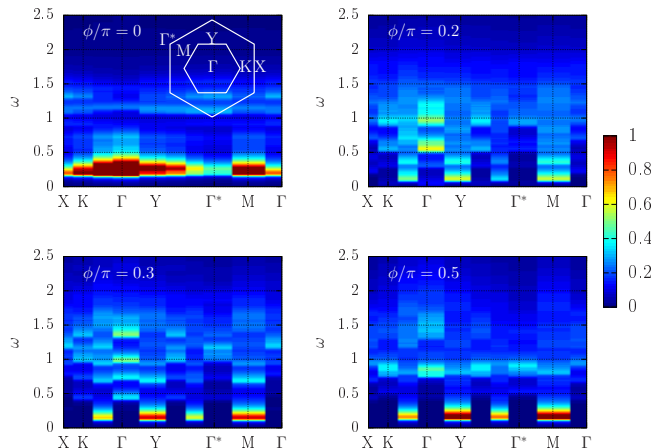


FIG. 10. Intensity plot of the dynamic structure factor, $S(\mathbf{q}, \omega)$, presented along high symmetry lines of the Brillouin zone for several values of ϕ , as obtained using the ED method. Pseudo-color indicates relative intensity. Inset: Brillouin zone with labels of symmetry points used in this figure.

V. DYNAMIC STRUCTURE FACTOR

A. Zero magnetic field

Next, we turn to spectral signatures of the $K - \Gamma$ spin liquid, which can be observed in experiments. The dynamic structure factor, which is probed in inelastic neutron scattering experiments, is defined as

$$S(\mathbf{q}, \omega) = \sum_{j,\alpha} \int dt \langle S_j^\alpha(t) S_0^\alpha(t=0) \rangle e^{-i\mathbf{q} \cdot (\mathbf{r}_j - \mathbf{r}_0) + i\omega t}. \quad (9)$$

We calculated $S(\mathbf{q}, \omega)$ using an ED method for a 24-site cluster, see appendix C for details. Fig. 10 shows $S(\mathbf{q}, \omega)$ for several values of ϕ . The first evident feature is the existence of a broad excitation continuum at high frequencies. In the Kitaev limit, $\Gamma = 0$, most of the spectral weight is found at relatively low energies, which is in agreement with literature^{29,30}. As Γ is increased, the low frequency spectral weight at the Brillouin zone center (Γ point) is pushed towards higher frequencies, while a low ω signal remains at the M, Y and $K/2$ (midway between K and Γ) points. In contrast to the spectra of the Kitaev-Heisenberg model^{38,39}, the spin gap at the Kitaev limit seems to remain finite even in the presence of large Γ . The difference in momentum dependence between high and low frequencies is clearly evident by integrating over different ranges of ω . In Fig. 11 we show the *relative* intensity of $S(\mathbf{q}, \omega)$, integrated over low and high frequency ranges. In the Kitaev limit, $\phi = 0$, $S(\mathbf{q}, \omega)$ is rather featureless. As

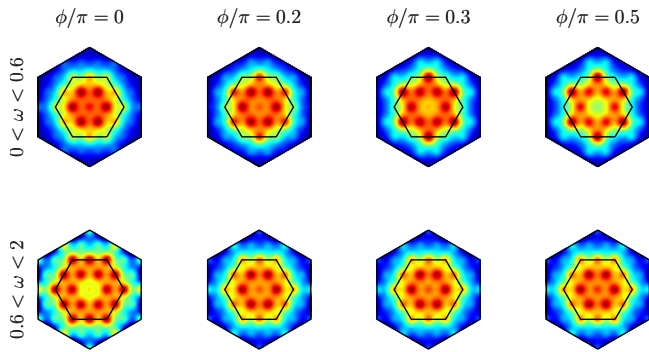


FIG. 11. Dynamical structure factor, $S(\mathbf{q}, \omega)$, integrated over low (top) and high (bottom) frequencies, as obtained from exact diagonalization. The discrete set of peaks in momentum space, resulting from the finite size of the studied cluster, was broadened in order to improve the visualization of the obtained pattern. The black lines depict the boundaries of the first and second Brillouin zones.

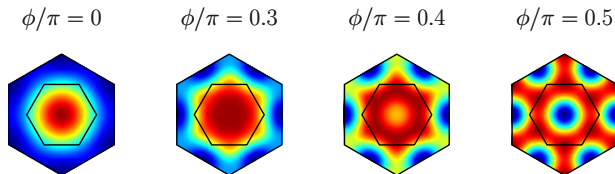


FIG. 12. Equal-time structure factor $S(\mathbf{q})$, obtained using the Majorana mean-field theory.

Γ is increased, $S(\mathbf{q}, \omega)$, integrated over a low frequency range, shows a star shaped pattern, similar to the pattern seen in the α -RuCl₃ neutron scattering experiments at low energies. In contrast, integrating over a range of higher frequencies, shows an almost featureless momentum dependence even for finite Γ , again, in qualitative agreement with the experiments.

To calculate the dynamic spin structure factor in the context of the Majorana MFT, one must consider Z_2 flux excitations with respect to the ground state, since each spin operator inserts a flux^{28,29}. Technically, this requires solutions to Eqns. (6) and (7) which go beyond the uniform ansatz considered here. It is however still possible to approximately calculate the equal-time spin structure factor,

$$S(\mathbf{q}) = \sum_{i,\alpha} \langle S_i^\alpha S_0^\alpha \rangle e^{-i\mathbf{q}\cdot(\mathbf{r}_i - \mathbf{r}_0)} \approx \frac{1}{4} \sum_{i,\alpha} \langle b_i^\alpha b_0^\alpha \rangle_B \langle c_i c_0 \rangle_A e^{-i\mathbf{q}\cdot(\mathbf{r}_i - \mathbf{r}_0)}. \quad (10)$$

Since $S(\mathbf{q}) = \int (d\omega/2\pi) S(\mathbf{q}, \omega)$, and noting that according to the ED results, most of the dynamic structure factor signal is concentrated at low frequencies, we ex-

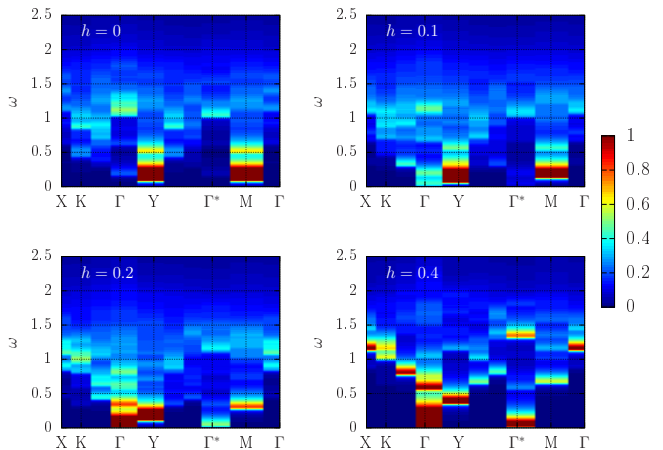


FIG. 13. Dynamic structure factor for $\phi/\pi = 0.2$, $J_3 = 0.05$, and several values of the magnetic field $h_{\perp c^*}$. Symmetry points labeled as in Fig. 10.

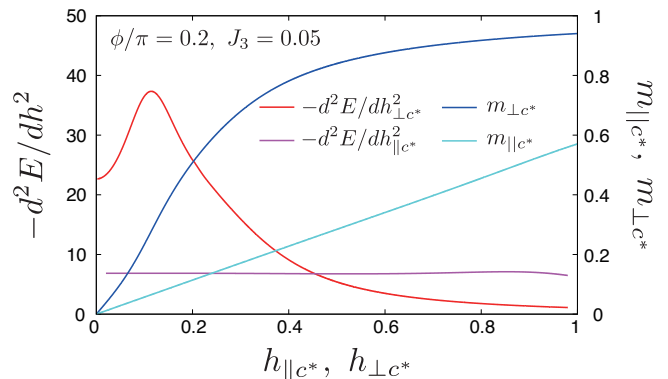


FIG. 14. Magnetization and second derivative of the energy as a function of magnetic field, parallel, $h_{\parallel c^*}$, and perpendicular, $h_{\perp c^*}$, to $c^* = (1, 1, 1)$.

pect that $S(\mathbf{q})$ resemble the integrated low frequency patterns of $S(\mathbf{q}, \omega)$. Indeed, as seen in Fig. 12, the mean-field theory reproduces the star shaped pattern seen both in experiments and in the ED calculation.

B. J_3 terms and finite magnetic field

Zig-zag magnetic ordering, similar to the magnetically ordered state observed in α -RuCl₃ at low temperatures, can be stabilized by adding a third neighbor Heisenberg term, $J_3 \sum_{\alpha, \langle ij \rangle \in 3^{\text{rd n.n.}}} S_i^\alpha S_j^\alpha$ to the Hamiltonian, Eq. (1). At this level, nearest neighbor Heisenberg terms are less important since microscopic calculations¹³ suggest that they are smaller, and J_3 is enough to stabilize the zig-zag magnetic order. Furthermore, it is possible to

suppress this ordering tendency by applying a magnetic field, $-\sum_{i\alpha} h^\alpha S_i^\alpha$. This is evident in Fig 13, which displays $S(\mathbf{q}, \omega)$ for $\phi/\pi = 0.2$, $J_3 = 0.05$ and several values of the in-plane magnetic field $h_{\perp c^*} \propto (-1, 1, 0)$, perpendicular to $c^* = (1, 1, 1)$, which corresponds to the out-of-plane direction. With $h_{\perp c^*} = 0$ the low ω spectral weight is increased at the M and Y points, but not at K/2. Notice, however, that most of the zone center (Γ point) spectral weight is found at relatively high energies¹⁵. This aspect of the spectra is similar to the case with $J_3 = 0$, $h = 0$, shown in Fig. 10. When $h_{\perp c^*}$ is increased beyond $h_{\perp c^*} \sim 0.1$, the zone center spectral weight shifts towards lower energies, and a continuum of excitations emerges.

Fig. 14 shows magnetization curves as obtained with ED, for magnetic fields pointing parallel, $h_{\parallel c^*}$, and perpendicular, $h_{\perp c^*}$, to c^* . A peak at $h_{\perp c^*} \sim 0.1$ in the second derivative of the energy $-d^2E/dh_{\perp c^*}^2$, indicates an apparent transition away from zig-zag order. In addition, the magnetization curves display an easy axis anisotropy, also consistent with α -RuCl₃ experiments^{16,17,40}. A simple mean-field analysis qualitatively explains the easy-plane anisotropy as follows: If a ferromagnetically ordered moment \vec{m} is assumed as a classical Weiss field, the mean-field energy E_{mf} is obtained as

$$\begin{aligned} E_{\text{mf}}/N &= -\frac{K - 3J_3}{2}(m_x^2 + m_y^2 + m_z^2) \\ &\quad + \Gamma(m_y m_z + m_z m_x + m_x m_y) \\ &= -\frac{K + \Gamma - 3J_3}{2}(m_x^2 + m_y^2 + m_z^2) \\ &\quad + \frac{\Gamma}{2}(m_x + m_y + m_z)^2, \end{aligned} \quad (11)$$

which is minimized, for finite $\Gamma > 0$, when $m_x + m_y + m_z = 0$ is satisfied, i.e., when the magnetic moments are in-plane.

VI. CONCLUSIONS

In this work, we investigated a spin model with both the Kitaev (K) and symmetric-anisotropic (Γ) interactions on the honeycomb lattice using iDMRG, exact diagonalization, and Majorana mean-field theory. This model is strongly motivated by recent experiments on α -RuCl₃, where K and Γ are likely to be the dominant exchange interactions.

We found strong numerical evidence for the existence of a quantum spin liquid for arbitrary ratio of Γ/K for ferro-like Kitaev interactions in iDMRG. In particular, the entanglement entropy remains very high in this entire region while we do not see any sign of magnetic order in iDMRG computations. In contrast, we found

a magnetically ordered state with very small entanglement entropy on the antiferro-like Kitaev side. Moreover, we demonstrated the existence of coherent two-dimensional multi-particle excitations using the correspondence between transfer-matrix eigenvalues and the lower boundary of multi-particle excitation spectrum. The cylinder geometry in iDMRG induces an anisotropy in bond-dependent energy, which is expected to move the locations in momentum space of low energy excitations. We show that this can indeed be seen in the transfer-matrix spectra. The existence of such two-dimensional coherence excitations without magnetic order is a very strong evidence of quantum spin liquid.

In order to make direct connection to neutron scattering experiments, we computed the dynamical structure factor for the $K - \Gamma$ model without and with a small third neighbor Heisenberg interaction J_3 using exact diagonalization of 24-site cluster. The J_3 on top of the $K - \Gamma$ interactions is shown to drive a transition to the zig-zag order in agreement with previous numerical studies^{13,15,22}. Upon introduction of Γ starting from the ferro-like Kitaev interaction, the dynamical structure factor develops the scattering continuum with star-like intensity profile at low energies, just like what is seen in recent neutron scattering experiment³. The magnetic field dependence of the dynamical structure factor is also investigated when J_3 is finite such that the ground state is the zig-zag magnetic order in zero field. There is a transition to a paramagnetic state with dominant scattering intensity at the zone center when the external magnetic field along the honeycomb plane reaches about 1/10 of the largest exchange interactions, namely K or Γ . This is seen in the magnetization profile and dynamical structure factor computed in exact diagonalization. All of these features are consistent with recent experimental data.

Further we used the Majorana mean-field theory to gain analytical insight in these numerical results. For example, we computed single and two-particle excitation spectra for the $K - \Gamma$ model showed they exhibit an emergent symmetry in their momentum dependence, which is also found in the transfer matrix spectrum. The equal-time structure factor and real-space spin correlations computed in the Majorana mean-field theory are also consistent with main features in the exact diagonalization results.

Combining all these results together, we conclude that the mysterious scattering continuum seen in the neutron scattering experiment on α -RuCl₃ may come from a nearby quantum spin liquid supported by $K - \Gamma$ interactions. In our numerical computations, the spin liquid phases at finite Γ/K show qualitatively the same behavior as the Kitaev spin liquid. We do see, however, a jump in the bond-dependent energy at some value of Γ/K in

iDMRG on cylinder geometry, which causes a small kink in the entanglement entropy. This can be interpreted as a meta-nematic transition, where the bond-anisotropy (or broken 3-fold rotation symmetry) increases abruptly. Whether such a transition would survive in the 2D limit is not clear to us at present. If it does survive, we would need to consider two possible scenarios. (i) The transfer matrix spectra on both sides of the transition share some qualitative features, suggesting that they are actually the same spin liquid phase, while the apparent transition may be interpreted as a Lifshitz transition on the Fermi surface topology of the underlying quasiparticles. (ii) Although the transfer matrix spectra may be described using Majorana fermions both before and after the transition, the underlying spin liquid ground states may be distinct. These questions will have to be addressed in future theoretical investigations. Further experimental data in external magnetic field would provide additional clues for the validity of the assumption that the $K - \Gamma$ or $K - \Gamma - J_3$ is a good minimal model for α -RuCl₃.

ACKNOWLEDGEMENTS

We would like to thank Andrei Catuneanu, Yin-Chen He, Masatoshi Imada, Hae-Young Kee, Young-June Kim, Stephen Nagler, Tsuyoshi Okubo, Natalia Perkins, Roser Valenti and Ruben Verresen for useful discussions. YY further thanks Mitsuaki Kawamura for his technical support. YY was supported by PRESTO, JST (JPMJPR15NF). The ED computation has partly been done using the facilities of the Supercomputer Center, the Institute for Solid State Physics, the University of Tokyo. MG and FP acknowledge support from the German Research Foundation (DFG) via SFB 1143 and Research Unit FOR 1807. GW and YBK are supported by the NSERC of Canada, Canadian Institute for Advanced Research, and the Center for Quantum Materials at the University of Toronto.

Appendix A: iDMRG and Transfer Matrix

This appendix is devoted to the infinite Density Matrix Renormalization (iDMRG) method and the transfer matrix spectrum. The first part exposes the geometry used in order to apply iDMRG onto a 2D lattice model. We present more in-depth discussion of possible finite size effects due to the finite circumference. The second part introduces the transfer matrix spectrum and its connection to the excitation spectrum.

Infinite Density Matrix Renormalization Group. We use iDMRG²³⁻²⁵ to study ground state properties of the

K- Γ model. Initially developed for 1D systems, it has been successfully applied on 2D systems by wrapping the lattice on a cylinder and mapping the cylinder to a chain. Furthermore employing translational invariance enables to study infinite cylinders^{24,25}. Using the cylinder geometry, one dimension of the lattice is finite and leads to a discretization of the related reciprocal vector. Thus, accessible momenta lie on lines in reciprocal space. We chose cylinder geometries, i.e. circumference L_{circ} and unit cell, such that the accessible momentum lines go through the gapless nodes of the isotropic Kitaev spin liquid, that are located at the K -points of the first Brillouin zone. The results presented here and in the main text are obtained using a rhombic unit cell and a narrow cylinder with $L_{circ} = 6$ sites circumference.

We extend the discussion of the main text by considering the average energy $\langle E_{x,y,z} \rangle$ of the x , y and z bonds for $0 \leq \phi \leq 0.5\pi$, which is presented in Fig. 6. In the limit of small Γ almost no anisotropy exists, which indicates negligible finite size effects caused by the cylinder geometry. Once Γ increases, the anisotropy raises and reaches $\max(\langle E_{y,z} \rangle / \langle E_x \rangle) \approx 2$ near $\phi = 0.3\pi$. Using wider cylinders with $L_{circ} = 12$ reduces the anisotropy only slightly. This suggests, that a Γ -like interaction is highly sensitive to finite size and a cylinder geometry and presumably causing the gapless Dirac nodes to shift away from the K -points in reciprocal space.

Transfer Matrix Spectrum. The transfer matrix (TM) of a wave function encoded as an infinite matrix product state (iMPS) contains full information about the static correlations²⁶. Intuitively, the TM translates the iMPS by a lattice vector along the chain in 1D or the cylinder in 2D. For Hamiltonians with only local interactions, the static correlations are related to the spectral gap⁴¹, e.g. $\xi \sim 1/\Delta$ for $z = 1$. This statement has been extended by Zauner et al.²⁶ to also include momentum, such that the length scale of the decay of static correlations with a momentum \mathbf{k} gives an upper bound on the spectral gap $\epsilon(\tilde{\mathbf{k}})$ at $\tilde{\mathbf{k}}$ close to \mathbf{k} . Hence, the TM spectrum, a ground state property, provides information about the position of the minimal energy excitation within the reciprocal space. A connection between the TM eigenvalues and the exact excitation energies can only be made knowing the Lieb-Robinson velocity⁴², e.g., from dynamics. Here, the Lieb-Robinson velocity is not known and thus the quasi-energies $E_i = -\log \lambda_i$, where λ_i are the eigenvalues of the TM, are *only* given up to an overall energy scale of the Hamiltonian.

On the cylinder geometry and If the symmetry upon translation along the cylinder's circumference is not broken, the transverse momentum k_y is a good quantum number. Then, for each k_y independently a set of λ_i exists with a longitudinal momentum $k_x = \arg \lambda_i$ corresponding to the momentum of minimal energy excita-

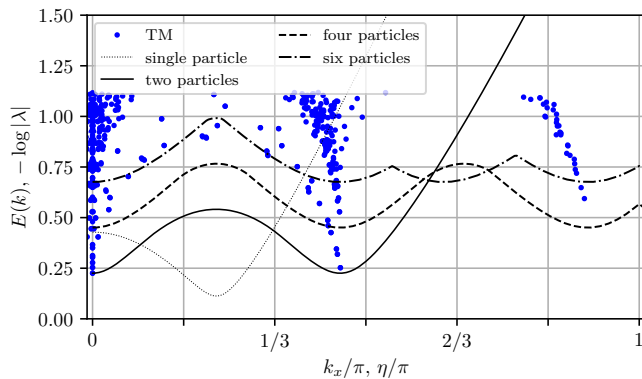


FIG. 15. Quasi-energies $E(k) = -\log \lambda_i$ of the *regular transfer matrix* spectrum λ_i compared to analytical excitation energies for single- (thin dotted), two- (solid), four- (dashed), and six-particle excitations (dash-dotted) of the anisotropic XY-Heisenberg chain with transverse field. The parameters are: $\gamma = 0.1$, $h = 0.75$. The analytical results are scaled by a factor $a = 1.73$ in order to match the $\min(E_i)$ with $\min(E_{2p}(k))$, where $E_{2p}(k)$ is the lower edge of the two-particle excitation band.

tion.

In Fig. 15 we illustrate an exemplary TM spectrum for the anisotropic XY-Heisenberg chain with transverse field h and anisotropy γ :

$$H = -J \sum_i [(1 + \gamma) S_i^x S_{i+1}^x + (1 - \gamma) S_i^y S_{i+1}^y + h S_i^z] , \quad (\text{A1})$$

This model can be solved exactly^{43–47} and its energy spectrum is known⁴⁷. The plot compares the TM spectrum $E_i(k_i) = -\log \lambda_i$ (blue dots) with the analytical single- and multi-particle excitations (lines). The position $k_i = \arg(\lambda_i)$ of the minimal eigenvalues E_i coincide nicely with the minimum in the excitation bands with an even number of particles. Single particle excitations are not present in the *regular* TM.

We provide a second example related to the model investigated in the main text. Taking the limit $\phi \rightarrow 0$ of eq. 1 one obtains the exactly solvable Kitaev model on a honeycomb lattice⁶. If the Kitaev couplings are isotropic $K_x = K_y = K_z$, the model exhibits gapless Dirac nodes at the K -points of the Brillouin zone. As long as $|K_\alpha| < |K_\beta| + |K_\gamma|$ with $\alpha, \beta, \gamma = \{x, y, z\}$, the excitation remain gapless. Once the K 's are tuned away from isotropy, the Dirac node moves and odd-numbered particle excitations get separated in reciprocal-space from even-numbered. Furthermore, the nodes may leave the allowed momenta cuts of the cylinder geometry introducing an effective gap. In Fig. 16 we present a comparison of the TM spectrum with analytical results for the single- and two-particle spectrum clearly illus-

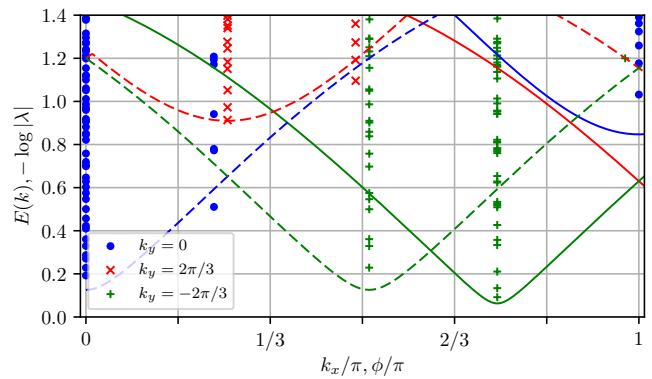


FIG. 16. Quasi-energies $E(k)$ of the anisotropic Kitaev model with $K_x = -1$, $K_y = -1.2$, and $K_z = -0.9$. Lines display the analytic results of the single-particle (solid) and two-particles (dashed) lowest energy excitation⁶ on the corresponding momentum cuts: $k_y = 0$ (blue), $k_y = 2\pi/3$ (red), and $k_y = -2\pi/3$ (green). The analytic results are scaled by a factor $a = 0.38$.

trating a correspondence between (k_x, k_y) of the TM eigenvalues and the minimum of the excitation bands. Remarkably, the TM spectrum recovers single-, three-, etc. particle excitations as well as two-, four-, etc. particle excitations.

The reader will find a more rigorous and detailed explanation as well as more examples in Zauner et al.²⁶.

Implementation. We turn now to the technical realization of obtaining the momentum resolved TM spectrum. Let λ_i be the eigenvalues of the transfer matrix with the ordering $|\lambda_0| > |\lambda_1| \geq |\lambda_2| \geq \dots$. By definition the dominant eigenvalue is $|\lambda_0| = 1$. Generally, λ_i are complex and can be decomposed as $\lambda_i = |\lambda_i| e^{i\eta}$. The angle η is connected to the momentum k_x along the chain or cylinder. Exploiting the rotational invariance of the Hamiltonian on the cylinder geometry yields the transverse momentum k_y as will be explained now. In the following, we require the iMPS to be in *canonical form*⁴⁸. A translation with a lattice vector along the circumference keeps the Hamiltonian invariant and as such k_y can be treated as a regular quantum number. We extract k_y by computing the dominant eigenvector $\tilde{\Lambda}_0$ of the *mixed* transfer matrix constructed out of the ground state iMPS and a iMPS with the translation applied, see also Fig. 17b). We like to remark, that the translation along the circumference is simply given by a permutation of sites within a ring. If the iMPS is sufficiently converged and the applied translation is indeed a symmetry, then the dominant eigenvalue $\tilde{\lambda}_0$ of the *mixed* TM is 1. Its eigenvector $\tilde{\Lambda}_0$ has a diagonal form with eigenvalues $|\tilde{\lambda}_i| e^{iq}$ and q being discretized in steps $2\pi/n$, where n is the number of unit cells around the

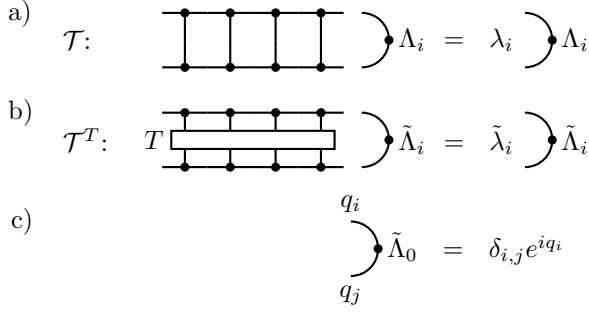


FIG. 17. Schematic representation of a) the *regular* and b) the *mixed* transfer matrix \mathcal{T} with translation T applied along the circumference. c) Dominant eigenvector $\tilde{\Lambda}_0$ of \mathcal{T}^T determines the q quantum numbers associated with each bond leg.

cylinder. If Schmidt values are degenerate, the diagonal form becomes block diagonal with blocks for each set of degenerate Schmidt values. Each block can be diagonalized separately by a unitary transformation which is then applied to the non-translated iMPS. The momentum quantum number q_i are associated with the entries i along a bond leg in the same way as Schmidt values are. The TM connects states i and j with corresponding q_i and q_j , hence the transverse momentum is given by $k_{y,(i,j)} = q_j - q_i$. The k_y label of λ_i can be read off from its eigenvector Λ_i due to the fact, that Λ_i has only non-zero entries with the same change of the quantum number $q_i - q_j$.

Anisotropic $K - \Gamma$ model. Here, we provide TM spectra in the case of anisotropic $K - \Gamma$ couplings in order to strengthen the discussion in the main text, section III B and IV B, about the symmetry of the b-fermions.

We introduce an anisotropy by scaling the coupling parameter $K_{\alpha}, \Gamma_{\alpha}$ by a factor a

$$\begin{aligned} (K_x, \Gamma_x) &\rightarrow (aK_x, a\Gamma_x) \\ (K_y, \Gamma_y) &\rightarrow ((3/2 - a/2)K_y, (3/2 - a/2)\Gamma_y) \\ (K_z, \Gamma_z) &\rightarrow ((3/2 - a/2)K_z, (3/2 - a/2)\Gamma_z), \end{aligned} \quad (\text{A2})$$

with respect to the x-bond. The anisotropy leads to a shift of the minimum in the c-fermion spectrum away from the K -point as is apparent in the MFT spectrum Fig. 20. The TM spectra, Fig. 18, do not display such a shift of the eigenvalues at the K -point (green +), neither for $\phi/\pi = 0.1$ nor for 0.35. Furthermore, the symmetry $\Omega_{\min.}(\mathbf{k} \pm \mathbf{K}) = \Omega_{\min.}(\mathbf{k})$ is unaffected by the anisotropy, which is consistent with the MFT prediction, App. B, for the b and the $b + c$ fermion spectrum.

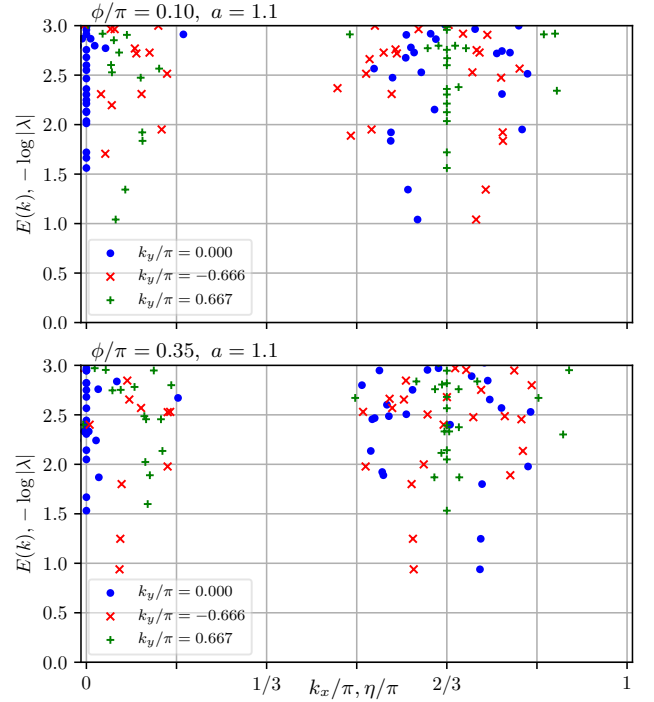


FIG. 18. Quasi-energies $E(k)$ of the anisotropic KT model for $\phi = 0.1$ (top) and $\phi = 0.35$ (bottom) with an anisotropy $a = 1.1$ according to eq. A2.

Appendix B: Majorana MFT details

Even before solving equations (6) and (7), it is important to characterize the behavior of the Majorana fermions under *any* configuration of A_{ij} and B_{ij} . The c_i operators describe fermions which move about the whole lattice with hopping amplitudes given by A_{ij} . Similarly, the b_i^α operators describe fermion hopping with amplitudes $B_{ij}K_{ij}^{\alpha\beta}$. Most importantly, the structure of $K_{ij}^{\alpha\beta}$, given in Eq. (4), separates the b_i^α fermions into three independent, uncorrelated sectors. Each sector is associated with one of the three sublattices of hexagons. Within each sector, the hopping amplitude is $B_{ij}\Gamma$ around a hexagon of the corresponding sublattice, and $B_{ij}K$ between neighboring hexagons. When $\Gamma = 0$, b_i^α fermions are bound to a bond, while they are bound to a hexagon when $K = 0$. This behavior echoes the macroscopic degeneracies of the parent classical models: in the classical Kitaev model there are a macroscopic number of degenerate ground states which are related to each other by reversing the sign of a single spin component for two spins on the same bond. The classical Γ -model has a similar macroscopic degeneracy, obtained by reversing the signs of one component of each

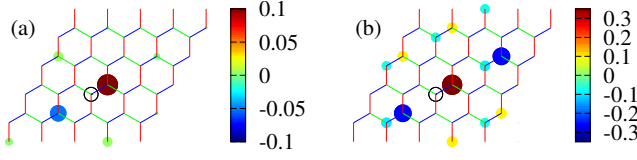


FIG. 19. Spin-spin correlations in real space. The open black circles indicate site $i = 0$ and the filled circles indicate i . The circle size and color represent the magnitude and value of the corresponding correlation $\langle S_i^x S_0^x \rangle$. (a) Mean-field results for $\phi/\pi = 0.4$. (b) ED results for $\phi/\pi = 0.5$. In both cases one finds same spin component correlations only among a subset of all sites.

of the six spins on one hexagon⁴⁹. Furthermore, returning to the uniform mean-field solution, the b -fermion band structure is similar to the band structure obtained in a Luttinger-Tisza study of the corresponding classical models, since both are determined by the exchange matrix $K_{ij}^{\alpha\beta}$. In the classical case, the flat bands for $\Gamma = 0$ or $K = 0$ indicate the existence of a macroscopic number of ground states, mentioned above.

Spin correlations in real space, shown in Fig. 19a, reveal a pattern which manifests the separation of b fermions into independent sectors: S_i^z on site i is correlated only with a certain subset of S_j^z 's on other sites j . Similar patterns are also obtained with ED, see Fig 19b although some differences should be pointed out. According to the MFT, at $\phi = 0.5$ ($K = 0$), there are non-zero spin-spin correlation only within the same hexagons since the b -fermions are localized. Thus, both finite K and Γ are required to get longer range correlations. Furthermore, the correlation in Fig. 19b don't decay very fast since they were obtained using ED on a small cluster with periodic boundary condition, whereas the correlations in 19a where calculating assuming an infinite system. Finally, even among the the subset of sites which have same spin component correlations, MFT gives nonzero *static* correlations only between opposite sublattice sites.

Next we show how the symmetry $\varepsilon_b(\mathbf{k} \pm \mathbf{K})$ emerges from the Majorana mean-field Hamiltonian, Eq. (5). We begin by assuming that the mean-field amplitudes B_{ij} preserve translational invariance, and inversion symmetry, but are not necessarily isotropic. We can therefore write the b -fermion Hamiltonian as

$$H_b = \sum_{\mathbf{k}} \sum_{L,L'=A,B} \sum_{\alpha\beta} K_{LL'}^{\alpha\beta}(\mathbf{k}) i b_L^\alpha(\mathbf{k}) b_{L'}^\beta(-\mathbf{k}), \quad (\text{B1})$$

where the Fourier transform of the b Majorana operators is

$$b_i = \frac{1}{\sqrt{N}} \sum_{\mathbf{k}} b_L(\mathbf{k}) e^{i\mathbf{k}\cdot\mathbf{r}_i}, \quad (\text{B2})$$

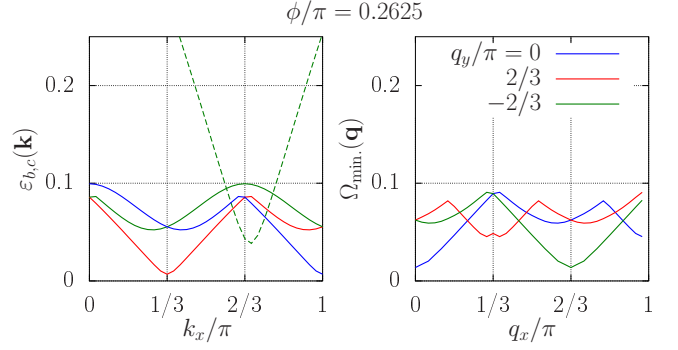


FIG. 20. Left: $\varepsilon_c(\mathbf{k})$ (dashed) and $\varepsilon_b(\mathbf{k})$ (solid) for anisotropic mean-field amplitudes $A_x = 1, A_y = 1.1, A_z = 1.2$ and $B_x = 0.45, B_y = 0.5, B_z = 0.55$. Right: minimum energy for $b + c$ excitations. The spectra are plotted along the allowed momentum cuts, as in Fig. 7.

and where $L = A, B$ denotes the sublattice of site i . The matrix $K_{LL'}^{\alpha\beta}(\mathbf{k})$ is the Fourier transform of $B_{ij} K_{ij}^{\alpha\beta}$, with $K_{ij}^{\alpha\beta}$ defined in Eq. (4). Thus, the sublattice off-diagonal block take the form

$$K_{AB}(\mathbf{k}) = \begin{pmatrix} K B_x T_1 & \Gamma B_z & \Gamma B_y T_2 \\ \Gamma B_z & K B_y T_2 & \Gamma B_x T_1 \\ \Gamma B_y T_2 & \Gamma B_x T_1 & K B_z \end{pmatrix}, \quad (\text{B3})$$

where $B_{x,y,z}$ are the anisotropic mean-field amplitudes, and $T_i = e^{i\mathbf{k}\cdot\mathbf{a}_i}$, with $\mathbf{a}_{1,2}$ the primitive lattice vectors for the honeycomb lattice. K itself is given by

$$K(\mathbf{k}) = \begin{pmatrix} & K_{AB}(\mathbf{k}) \\ K_{AB}^\dagger(\mathbf{k}) & \end{pmatrix}. \quad (\text{B4})$$

Under a shift in momentum $\mathbf{k} \rightarrow \mathbf{k} \pm \mathbf{K}$, $T_1 \rightarrow T_1 \eta$ and $T_2 \rightarrow T_2 \eta^*$, where $\eta = e^{2\pi i/3}$. Using the phases η we next observe that

$$K_{AB}(\mathbf{k}) = \begin{pmatrix} 1 & & \\ & \eta^* & \\ & & \eta \end{pmatrix} K_{AB}(\mathbf{k} \pm \mathbf{K}) \begin{pmatrix} \eta & & \\ & 1 & \\ & & \eta^* \end{pmatrix}. \quad (\text{B5})$$

The above relation shows that there exists a unitary transformation which takes $K(\mathbf{k} \pm \mathbf{K}) \rightarrow K(\mathbf{k})$, and therefore, the spectrum at the shifted momentum must be the same. As noted in the main text, this symmetry holds irrespective of the details of the c fermion spectrum, and is therefore always induced in the $b + c$ spectrum as well. Fig. 20 shows the single and two particle spectrum with fully anisotropic mean-field couplings. The minimum in the c fermions spectrum is clearly shifted away from the K point ($2\pi/3, -2\pi/3$), while the $b + c$ spectrum still exhibits the symmetry $\Omega_{\min.}(\mathbf{k} \pm \mathbf{K}) = \Omega_{\min.}(\mathbf{k})$. Finally, in Fig. 21 we use

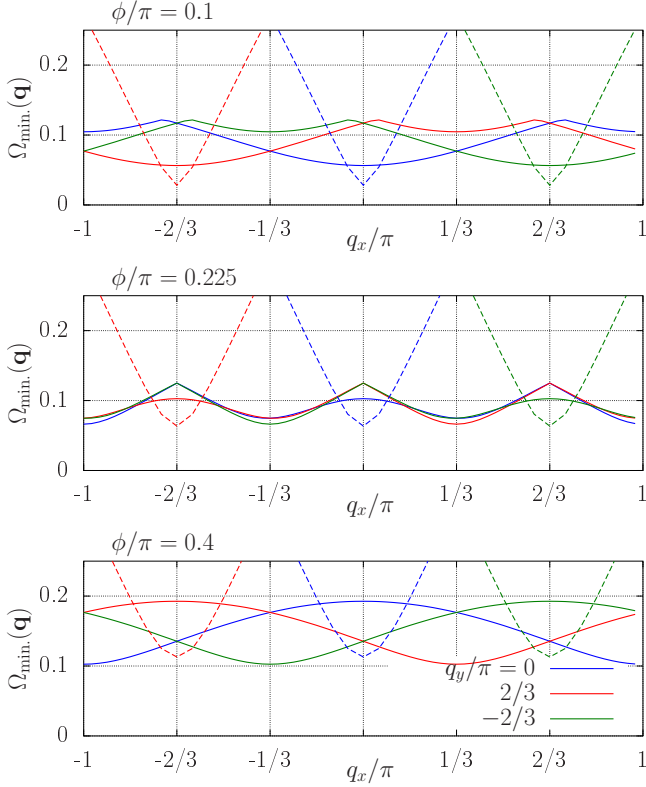


FIG. 21. $\Omega_{\min}(\mathbf{q})$ for $c+c$ (dashed) and $b+c$ (solid) excitations, plotted along the momentum cuts in Fig. 7 for different values of ϕ .

the mean-field Hamiltonian, Eq. (5), to demonstrate, that the soft modes in the two-particle spectrum move in momentum space, as ϕ is increased.

Appendix C: Dynamical structure factors and the Krylov subspace method

The dynamical structure factor may be written as

$$S(\vec{Q}, \omega) = \sum_{\alpha=x,y,z} S^{\alpha\alpha}(\vec{Q}, \omega), \quad (\text{C1})$$

where

$$S^{\alpha\alpha}(\vec{Q}, \omega) = -\frac{1}{\pi} \text{Im} \langle 0 | \hat{S}_{-\vec{Q}}^{\alpha} \frac{1}{\omega + i\delta - \hat{H} + E_0} \hat{S}_{+\vec{Q}}^{\alpha} | 0 \rangle, \quad (\text{C2})$$

and $\vec{S}_{+\vec{Q}} = (\hat{S}_{+\vec{Q}}^x, \hat{S}_{+\vec{Q}}^y, \hat{S}_{+\vec{Q}}^z)$ is the Fourier transform of the spin operators \vec{S}_i defined as,

$$\vec{S}_{\vec{Q}} = N^{-1/2} \sum_i \vec{S}_i e^{+i\vec{Q} \cdot \vec{r}_i}. \quad (\text{C3})$$

The dynamical structure factors are conventionally calculated by using the Lanczos algorithm initialized with an excited state $\hat{S}_{+\vec{Q}}^{\alpha} | 0 \rangle$ ^{50,51}. However, naive implementations of the Lanczos algorithm and continued fraction⁵⁰ requires careful examination of the convergence of excited states relevant to the spectra to control the truncation errors. In contrast, modern Krylov subspace methods, which extract essence from the Lanczos algorithm, offer controlled convergence without additional numerical costs.

Here, we solve a linear equation by employing a conjugate gradient (CG) method, instead of explicitly calculating the resolvent of \hat{H} in Eq.(C2). The CG methods find the solution in a Krylov subspace, as follows. First, by introducing the following two vectors,

$$|\chi(\zeta)\rangle = (\zeta - \hat{H})^{-1} \hat{S}_{+\vec{Q}}^{\alpha} | 0 \rangle, \quad (\text{C4})$$

$$|\phi\rangle = \hat{S}_{+\vec{Q}}^{\alpha} | 0 \rangle \quad (\text{C5})$$

we rewrite $S^{\alpha\alpha}(\vec{Q}, \omega)$ as

$$S^{\alpha\alpha}(\vec{Q}, \omega) = -\frac{1}{\pi} \text{Im} \langle \phi | \chi(\omega + i\delta) \rangle. \quad (\text{C6})$$

To obtain the unknown vector $|\chi(\zeta)\rangle$, we solve the following linear equation,

$$(\zeta - \hat{H}) |\chi(\zeta)\rangle = |\phi\rangle. \quad (\text{C7})$$

When the linear dimension of the matrix \hat{H} , \mathcal{L} , is too large to store the whole matrix in the memory, the linear equation is solved iteratively, for example, by using the CG methods. At n th iteration, the conjugate gradient algorithm initialized with $|\chi_0(\zeta)\rangle = |\phi\rangle$ finds an approximate solution $|\chi_n(\zeta)\rangle$ within a n -dimensional Krylov subspace $\mathcal{K}_n(\zeta - \hat{H}, |\phi\rangle) = \text{span}\{|\phi\rangle, (\zeta - \hat{H})|\phi\rangle, \dots, (\zeta - \hat{H})^{n-1}|\phi\rangle\}$. At each steps, the CG-type algorithms search the approximate solution $|\chi_n(\zeta)\rangle$ to minimize the 2-norm of the residual vector,

$$|\rho_n(\zeta)\rangle = (\zeta - \hat{H}) |\chi_n(\zeta)\rangle - |\phi\rangle. \quad (\text{C8})$$

We note that one needs to solve Eq.(C7) essentially once at a fixed complex number $\zeta = \omega + i\delta$ to obtain whole spectrum $S^{\alpha\alpha}(\vec{Q}, \omega)$. Due to the shift invariance of the Krylov subspace⁵², namely, $\mathcal{K}_n(\zeta - \hat{H}, |\phi\rangle) = \mathcal{K}_n(\zeta' - \hat{H}, |\phi\rangle)$ for any complex number $\zeta' \neq \zeta$, we can

obtain $|\chi(\zeta')\rangle$ from $|\chi(\zeta)\rangle$ with a numerical complexity of $\mathcal{O}(\mathcal{L}^0)^{52}$. The Krylov subspace methods utilizing the shift invariance are called the shifted Krylov subspace methods.

For the calculations of $S(\vec{Q}, \omega)$, we employ the shifted biconjugate gradient (BiCG) method implemented in a numerical library $K\omega$ for the shifted Krylov subspace method⁵³. The condition for truncating the shifted

BiCG iteration is set $\max_{\omega} \{ \|\rho_n(\omega + i\delta)\| \} < 10^{-4}$ for the following calculations with $\delta = 0.02$. The number of the iteration steps for satisfying the condition depends on the parameters (ϕ , J_3 , and B), and is typically of the order of one thousand and at most of the order of ten thousand.

-
- ¹ Leon Balents, “Spin liquids in frustrated magnets,” *Nature* **464**, 199–208 (2010).
- ² A. Banerjee, C. A. Bridges, J.-Q. Yan, A. A. Aczel, L. Li, M. B. Stone, G. E. Granroth, M. D. Lumsden, Y. Yiu, J. Knolle, S. Bhattacharjee, D. L. Kovrizhin, R. Moessner, D. A. Tennant, D. G. Mandrus, and S. E. Nagler, “Proximate Kitaev quantum spin liquid behaviour in a honeycomb magnet,” *Nature Materials* **15**, pages 733740 (2016).
- ³ Arnab Banerjee, Jiaqiang Yan, Johannes Knolle, Craig A. Bridges, Matthew B. Stone, Mark D. Lumsden, David G. Mandrus, David A. Tennant, Roderich Moessner, and Stephen E. Nagler, “Neutron scattering in the proximate quantum spin liquid α -RuCl₃,” *Science* **356**, 1055–1059 (2017).
- ⁴ Kejing Ran, Jinghui Wang, Wei Wang, Zhao-Yang Dong, Xiao Ren, Song Bao, Shichao Li, Zhen Ma, Yuan Gan, Youtian Zhang, J. T. Park, Guochu Deng, S. Danilkin, Shun-Li Yu, Jian-Xin Li, and Jinsheng Wen, “Spin-Wave Excitations Evidencing the Kitaev Interaction in Single Crystalline α -RuCl₃,” *Phys. Rev. Lett.* **118**, 107203 (2017).
- ⁵ K. W. Plumb, J. P. Clancy, L. J. Sandilands, V. V. Shankar, Y. F. Hu, K. S. Burch, Hae-Young Kee, and Young-June Kim, “ α -RuCl₃: A spin-orbit assisted Mott insulator on a honeycomb lattice,” *Phys. Rev. B* **90**, 041112 (2014).
- ⁶ Alexei Kitaev, “Anyons in an exactly solved model and beyond,” *Annals of Physics* **321**, 2–111 (2006).
- ⁷ G. Jackeli and G. Khaliullin, “Mott Insulators in the Strong Spin-Orbit Coupling Limit: From Heisenberg to a Quantum Compass and Kitaev Models,” *Phys. Rev. Lett.* **102**, 017205 (2009).
- ⁸ William Witczak-Krempa, Gang Chen, Yong Baek Kim, and Leon Balents, “Correlated Quantum Phenomena in the Strong Spin-Orbit Regime,” *Annual Review of Condensed Matter Physics* **5**, 57–82 (2014).
- ⁹ Jeffrey G. Rau, Eric Kin-Ho Lee, and Hae-Young Kee, “Spin-orbit physics giving rise to novel phases in correlated systems: Iridates and related materials,” *Annual Review of Condensed Matter Physics* **7**, 195–221 (2016).
- ¹⁰ Stephen M. Winter, Alexander A. Tsirlin, Maria Daghofer, Jeroen van den Brink, Yogesh Singh, Philipp Gegenwart, and Roser Valenti, “Models and Materials for Generalized Kitaev Magnetism,” *Journal of Physics: Condensed Matter* **29**, 493002 (2017).
- ¹¹ S. Trebst, “Kitaev Materials,” ArXiv e-prints (2017), arXiv:1701.07056 [cond-mat.str-el].
- ¹² Jeffrey G. Rau, Eric Kin-Ho Lee, and Hae-Young Kee, “Generic Spin Model for the Honeycomb Iridates beyond the Kitaev Limit,” *Phys. Rev. Lett.* **112**, 077204 (2014).
- ¹³ Stephen M. Winter, Ying Li, Harald O. Jeschke, and Roser Valenti, “Challenges in design of Kitaev materials: Magnetic interactions from competing energy scales,” *Phys. Rev. B* **93**, 214431 (2016).
- ¹⁴ Heung-Sik Kim and Hae-Young Kee, “Crystal structure and magnetism in α -RuCl₃: An ab initio study,” *Phys. Rev. B* **93**, 155143 (2016).
- ¹⁵ Stephen M. Winter, Kira Riedl, Andreas Honecker, and Roser Valenti, “Breakdown of magnons in a strongly spin-orbital coupled magnet,” *Nature Communications* **8**, 1152 (2017).
- ¹⁶ R. D. Johnson, S. C. Williams, A. A. Haghighirad, J. Singleton, V. Zapf, P. Manuel, I. I. Mazin, Y. Li, H. O. Jeschke, R. Valenti, and R. Coldea, “Monoclinic crystal structure of α -RuCl₃ and the zigzag antiferromagnetic ground state,” *Phys. Rev. B* **92**, 235119 (2015).
- ¹⁷ J. A. Sears, M. Songvilay, K. W. Plumb, J. P. Clancy, Y. Qiu, Y. Zhao, D. Parshall, and Young-June Kim, “Magnetic order in α -RuCl₃: A honeycomb-lattice quantum magnet with strong spin-orbit coupling,” *Phys. Rev. B* **91**, 144420 (2015).
- ¹⁸ A. Little, Liang Wu, P. Lampen-Kelley, A. Banerjee, S. Patankar, D. Rees, C. A. Bridges, J.-Q. Yan, D. Mandrus, S. E. Nagler, and J. Orenstein, “Antiferromagnetic Resonance and Terahertz Continuum in α -RuCl₃,” *Phys. Rev. Lett.* **119**, 227201 (2017).
- ¹⁹ M. Gohlke, R. Verresen, R. Moessner, and F. Pollmann, “Dynamics of the Kitaev-Heisenberg Model,” *Phys. Rev. Lett.* **119**, 157203 (2017).
- ²⁰ Wei Wang, Zhao-Yang Dong, Shun-Li Yu, and Jian-Xin Li, “Theoretical investigation of magnetic dynamics in α -RuCl₃,” *Phys. Rev. B* **96**, 115103 (2017).
- ²¹ Masahiko G. Yamada, Hiroyuki Fujita, and Masaki Oshikawa, “Designing Kitaev Spin Liquids in Metal-Organic Frameworks,” *Physical Review Letters* **119**, 057202 (2017).
- ²² Andrei Catuneanu, Youhei Yamaji, Gideon Wachtel, Hae-Young Kee, and Yong Baek Kim, “Realizing quantum spin liquid phases in spin-orbit driven correlated materials,” arXiv:1701.07837 [cond-mat] (2017).
- ²³ Steven R. White, “Density matrix formulation for quan-

- tum renormalization groups,” *Phys. Rev. Lett.* **69**, 2863–2866 (1992).
- ²⁴ I. P. McCulloch, “Infinite size density matrix renormalization group, revisited,” arXiv:0804.2509 [cond-mat] (2008).
- ²⁵ Jonas A. Kjäll, Michael P. Zaletel, Roger S. K. Mong, Jens H. Bardarson, and Frank Pollmann, “Phase diagram of the anisotropic spin-2 XXZ model: Infinite-system density matrix renormalization group study,” *Phys. Rev. B* **87**, 235106 (2013).
- ²⁶ V. Zauner, D. Draxler, L. Vanderstraeten, M. Degroote, J. Haegeman, M. M. Rams, V. Stojevic, N. Schuch, and F. Verstraete, “Transfer matrices and excitations with matrix product states,” *New J. Phys.* **17**, 053002 (2015).
- ²⁷ Yin-Chen He, Michael P. Zaletel, Masaki Oshikawa, and Frank Pollmann, “Signatures of Dirac Cones in a DMRG Study of the Kagome Heisenberg Model,” *Physical Review X* **7**, 031020 (2017).
- ²⁸ G. Baskaran, Saptarshi Mandal, and R. Shankar, “Exact Results for Spin Dynamics and Fractionalization in the Kitaev Model,” *Phys. Rev. Lett.* **98**, 247201 (2007).
- ²⁹ J. Knolle, D.L. Kovrizhin, J.T. Chalker, and R. Moessner, “Dynamics of a Two-Dimensional Quantum Spin Liquid: Signatures of Emergent Majorana Fermions and Fluxes,” *Phys. Rev. Lett.* **112**, 207203 (2014).
- ³⁰ J. Knolle, D. L. Kovrizhin, J. T. Chalker, and R. Moessner, “Dynamics of fractionalization in quantum spin liquids,” *Phys. Rev. B* **92**, 115127 (2015).
- ³¹ Ravi Yadav, Nikolay A. Bogdanov, Vamshi M. Katukuri, Satoshi Nishimoto, Jeroen van den Brink, and Liviu Hozoi, “Kitaev exchange and field-induced quantum spin-liquid states in honeycomb α - RuCl_3 ,” *Scientific Reports* **6**, 37925 (2016).
- ³² S.-H. Baek, S.-H. Do, K.-Y. Choi, Y. S. Kwon, A. U. B. Wolter, S. Nishimoto, Jeroen van den Brink, and B. Büchner, “Evidence for a Field-Induced Quantum Spin Liquid in α - RuCl_3 ,” *Physical Review Letters* **119**, 037201 (2017).
- ³³ Richard Hentrich, Anja U. B. Wolter, Xenophon Zotos, Wolfram Brenig, Domenic Nowak, Anna Isaeva, Thomas Doert, Arnab Banerjee, Paula Lampen-Kelley, David G. Mandrus, Stephen E. Nagler, Jennifer Sears, Young-June Kim, Bernd Büchner, and Christian Hess, “Large field-induced gap of Kitaev-Heisenberg paramagnons in α - RuCl_3 ,” arXiv:1703.08623 [cond-mat] (2017).
- ³⁴ Jiacheng Zheng, Kejing Ran, Tianrun Li, Jinghui Wang, Pengshuai Wang, Bin Liu, Zheng-Xin Liu, B. Normand, Jinsheng Wen, and Weiqiang Yu, “Gapless Spin Excitations in the Field-Induced Quantum Spin Liquid Phase of α - RuCl_3 ,” *Phys. Rev. Lett.* **119**, 227208 (2017).
- ³⁵ J. A. Sears, Y. Zhao, Z. Xu, J. W. Lynn, and Young-June Kim, “Phase diagram of α - RuCl_3 in an in-plane magnetic field,” *Physical Review B* **95**, 180411 (2017).
- ³⁶ A. U. B. Wolter, L. T. Corredor, L. Janssen, K. Nenkov, S. Schönecker, S.-H. Do, K.-Y. Choi, R. Albrecht, J. Hunger, T. Doert, M. Vojta, and B. Büchner, “Field-induced quantum criticality in the Kitaev system α - RuCl_3 ,” *Physical Review B* **96**, 041405 (2017).
- ³⁷ Zhe Wang, S. Reschke, D. Hüvonen, S.-H. Do, K.-Y. Choi, M. Gensch, U. Nagel, T. Rößm, and A. Loidl, “Magnetic Excitations and Continuum of a Possibly Field-Induced Quantum Spin Liquid in α - RuCl_3 ,” *Phys. Rev. Lett.* **119**, 227202 (2017).
- ³⁸ Youhei Yamaji, Takafumi Suzuki, Takuto Yamada, Seiichiro Suga, Naoki Kawashima, and Masatoshi Imada, “Clues and criteria for designing a Kitaev spin liquid revealed by thermal and spin excitations of the honeycomb iridate Na_2IrO_3 ,” *Phys. Rev. B* **93**, 174425 (2016).
- ³⁹ Dorota Gotfryd, Juraj Rusnačko, Krzysztof Wohlfeld, George Jackeli, Jiří Chaloupka, and Andrzej M. Oleś, “Phase diagram and spin correlations of the Kitaev-Heisenberg model: Importance of quantum effects,” *Phys. Rev. B* **95**, 024426 (2017).
- ⁴⁰ Lukas Janssen, Eric C. Andrade, and Matthias Vojta, “Magnetization processes of zigzag states on the honeycomb lattice: Identifying spin models for α - RuCl_3 and Na_2IrO_3 ,” *Physical Review B* **96**, 064430 (2017).
- ⁴¹ M. B. Hastings, “Locality in Quantum and Markov Dynamics on Lattices and Networks,” *Phys. Rev. Lett.* **93**, 140402 (2004).
- ⁴² E. Lieb and D. W. Robinson, “The finite group velocity of quantum spin systems,” *Commun.Math. Phys.* **28**, 251–257 (1972).
- ⁴³ E. Lieb, T. Schultz, and D. Mattis, “Two soluble models of an antiferromagnetic chain,” *Annals of Physics* **16**, 407–466 (1961).
- ⁴⁴ S. Katsura, “Statistical Mechanics of the Anisotropic Linear Heisenberg Model,” *Phys. Rev.* **127**, 1508–1518 (1962).
- ⁴⁵ Eytan Barouch, Barry M. McCoy, and Max Dresden, “Statistical Mechanics of the XY Model. I,” *Phys. Rev. A* **2**, 1075–1092 (1970).
- ⁴⁶ Eytan Barouch and Barry M. McCoy, “Statistical Mechanics of the XY Model. II. Spin-Correlation Functions,” *Phys. Rev. A* **3**, 786–804 (1971).
- ⁴⁷ U. Schmidt, “The Excitation Spectrum of the One-dimensional XY-Model in a Magnetic Field,” *Z. Physik* **267**, 271–275 (1974).
- ⁴⁸ Guifré Vidal, “Efficient Classical Simulation of Slightly Entangled Quantum Computations,” *Phys. Rev. Lett.* **91**, 147902 (2003).
- ⁴⁹ Ioannis Rousochatzakis and Natalia B. Perkins, “Classical Spin Liquid Instability Driven By Off-Diagonal Exchange in Strong Spin-Orbit Magnets,” *Physical Review Letters* **118**, 147204 (2017).
- ⁵⁰ E. R. Gagliano and C. A. Balseiro, “Dynamical Properties of Quantum Many-Body Systems at Zero Temperature,” *Phys. Rev. Lett.* **59**, 2999–3002 (1987).
- ⁵¹ Elbio Dagotto, “Correlated electrons in high-temperature superconductors,” *Rev. Mod. Phys.* **66**, 763–840 (1994).
- ⁵² Andreas Frommer, “Bicgstab (ℓ) for families of shifted linear systems,” *Computing* **70**, 87–109 (2003).
- ⁵³ A numerical library for the shifted Krylov methods, $K\omega$, developed by M. Kawamura based on Refs.54 and 55, is available through <https://github.com/issp-center-dev/Komega>.
- ⁵⁴ Tomohiro Sogabe, Takeo Hoshi, Shao-Liang Zhang, and Takeo Fujiwara, “A numerical method for calculating the

Green's function arising from electronic structure theory," in *Frontiers of Computational Science* (Springer, 2007) pp. 189–195.

⁵⁵ Susumu Yamamoto, Tomohiro Sogabe, Takeo Hoshi,

Shao-Liang Zhang, and Takeo Fujiwara, "Shifted conjugate-orthogonalconjugate-gradient method and its application to double orbital extended Hubbard model," *Journal of the Physical Society of Japan* **77**, 114713 (2008).